Mathematics and Systems Science 2025, 3(2), 3059.
https://doi.org/10.54517/mss3059

Article

Fractal behavior accompanied by the complex-conjugated power-law exponents discovered in living systems: Analysis of the temporal evolution of impedance in silkworm cocoons

Raoul R. Nigmatullin[1], Moupali Chakraborty[2], Karabi Biswas[3,*]

[1] Radioelectronics and Informative-Measurements Techniques Department, Kazan National Research Technical University (KNITU-KAI) named by A.N. Tupolev, 420111 Kazan, Russia
[2] Faculty of Engineering, Computing and the Environment, Kingston University London, London SW15 3DW, United Kingdom
[3] Department of Electrical Engineering, Indian Institute of Technology Kharagpur, Kharagpur 721302, India
*** Corresponding author:** Karabi Biswas, karabi@ee.iitkgp.ac.in

CITATION

Nigmatullin RR, Chakraborty M, Biswas K. Fractal behavior accompanied by the complex-conjugated power-law exponents discovered in living systems: Analysis of the temporal evolution of impedance in silkworm cocoons. Mathematics and Systems Science. 2025; 3(2): 3059. https://doi.org/10.54517/mss3059

ARTICLE INFO

Received: 11 November 2024
Accepted: 17 March 2025
Available online: 15 April 2025

Abstract: In this paper, we continue using the theoretical model describing 3D-branching systems that is applied to describe the living system, such as the silkworm butterfly cocoons (Bombyx mori). The proposed fitting function that follows from the applied model allows us to describe completely with high accuracy (the fitting error is less than 0.1%) the whole stage of the temporal evolution of the silkworm cocoons in room conditions (during 13 days of the experiment the lowest temperature noted was 27 ℃ and the highest temperature was 29 ℃) and with relative humidity located in the interval [$H_{\min}$ 54% ≤ H ≤ 76% $H_{\max}$] during 13 days (13 November 2023 to 25 November 2023) of the impedance measurements. The selection of this biological object is related to the fact that all possible conducting channels formed inside the given cocoon have 3D structures. Analysis of the measured impedance data shows that the measurements at the beginning of each day have a monotone character, while each measurement after the first measurement of each day has chaotic behavior. It means that during the night a cocoon "has a rest". After this resting period, the applied voltage disturbs internal processes that are reflected in the behavior of the measured impedance. It has an oscillating character. These oscillations reflect the "regrouping" of conducting channels that take place inside the measured cocoon.

Keywords: 3D-branching/fractal systems; impedance measurements in silkworm cocoons; new fractal element with complex-conjugated power-law exponents in 3D systems

1. Introduction

The mathematical model describing 3D-branching systems of a complex living system is the continuation of the previous modeling of leaves and mushrooms [1,2]. A whole stage of the temporal evolution of the silkworm cocoons in room conditions and with relative humidity has been examined by analyzing the impedance of cocoons for 13 days. Silkworm cocoons, most commonly Bombyx mori, are human-cultivated composite materials that are known as the commercial source of silk [3,4]. Apart from silk production, Bombyx mori is frequently used as a research model in life science [5], drug discovery, antiviral agents [6], environmental and food safety [7], drug screening [8], and toxicological research [9,10]. Researchers also produced electricity from the cocoon membrane. Tulachan et al. show that a dry cocoon behaves as an insulator, whereas it generates an electrical current when it is exposed to moisture [11]. Silk-based materials for biomedical applications are gaining momentum as a research topic [12,13].

In this paper, a novel 3D-structured conducting channel is discovered inside the cocoon, and a mathematical model of the 3D branching is explained with the complex conjugated power law of exponents. The total number of impedance measurements equals 76. The detailed time intervals of these experiments are shown in **Table 1**. The set of these experimental measurements covers all stages associated with the transformation of a "freshly" formed cocoon to the adult silkworm moth. The other three days are associated with the adult moth sitting on the cocoon shell after coming out from it. The fitting parameters that follow from the model enable the demonstration of at least three stages. These stages are seen in **Figure 1**.

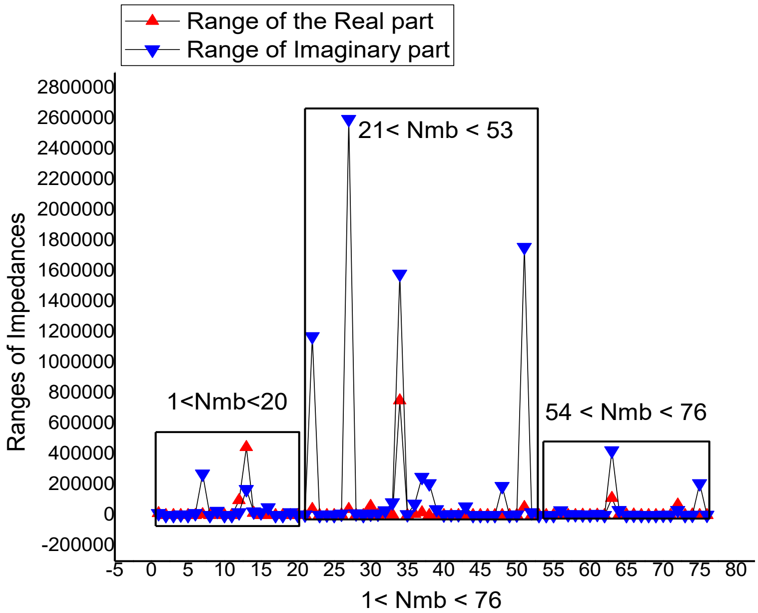

Figure 1. The real and imaginary parts of the measured impedance data.

This figure demonstrates the distribution of the ranges corresponding to real (red triangles) and imaginary (blue triangles) impedances, correspondingly. One can select approximately at least three regions where the values of impedances are different from each other. They are closed in the corresponding rectangles.

2. Experimental details

This section describes the experiments carried out with the cocoon of the silk fly. 25 numbers of two-day-old cocoons are collected from the Debra Sericulture Department, Debra, West Medinipur, India. In **Figure 2a**, the electrode connection is shown. Two gold electrodes are connected at the two ends (lengthwise) of the cocoon. To keep the position fixed, it is inserted inside a perforated plastic tube and placed on a petri dish using thermocol packing (**Figure 2b**). The remaining cocoons are kept in the same environmental condition on a different petri dish, and no excitation is applied to them. In **Figure 2c**, the pupa inside the cocoon can be seen.

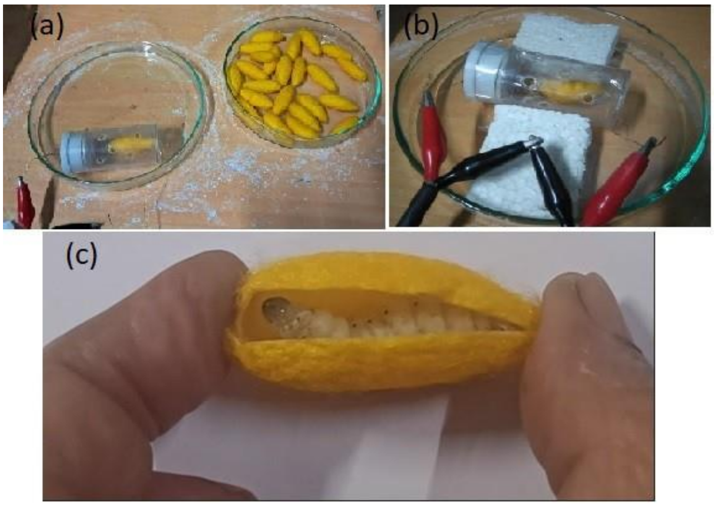

Figure 2. Photograph of the electrode connection and experimental set-up at the start of the experiment. **(a)** Photograph of fresh cocoons; **(b)** cocoon with electrical connection for impedance measurement; **(c)** photograph of the living pupa inside the cocoon's shell.

The experiments were conducted for 13 days. A sinusoidal excitation of amplitude 0.5 V is applied to the electrodes connected to the shell using an impedance analyzer (make: Novocontrol, model: Alpha A). The frequency is varied from 4 MHz to 10 mHz and impedance is noted at 86 points equally distributed to the frequency range. After 10 days, the moth (the white-colored one sitting on the yellow-colored shell) came out from one side of the shell, as can be seen in **Figure 3a**. At the same time, the moths from the other cocoons that were not under test also came out (**Figure 3b**). That means the cocoon under test and the other cocoons had taken the same time for the evolution from pupa to silk-fly. The experiment was continued for 3 more days while the silk fly was sitting on the broken shell. The experimentally obtained impedance data is provided in **Table 1**.

Figure 3. Photograph of the moth that came out of the shell after the 10th day of the start of the experiment. **(a)** White-colored moth came out of the cocoon which was under test; **(b)** moths that came out of the cocoons which were not under test.

Experiments were conducted inside a controlled laboratory environment, and the humidity and temperature were noted at the beginning of each trigger given to the cocoon. The temperature varied between 27 ℃ and 29 ℃. The relative humidity noted was between 54% and 76%.

Table 1. The distribution of the impedance measurements over the overall period.

Day	Time	Time	Time	Time	Time	Time	Time	Number of experiments
13.11	7.45	9.00	10.00	-	-	-	-	3
14.11	10.20	11.45	12.45	16.15	18.00	-	-	5
15.11	11.00	12.30	13.45	16.30	17.45	19.15	20.30	7
16.11	10.45	12.00	13.30	15.45	17.15	19.00	20.30	7
17.11	10.45	12.00	13.30	15.45	17.15	18.45	-	6
18.11	10.30	12.00	13.40	16.00	17.00	19.00	-	6
19.11	10.15	11.45	13.25	16.45	18.15	19.45	-	6
20.11	9.45	11.30	13.00	14.45	16.15	18.00	19.30	7
21.11	10.15	11.45	13.15	14.45	16.15	18.00	20.00	7
22.11	10.30	11.45	13.00	14.30	17.00	-	-	5
23.11	10.00	11.30	13.00	15.45	17.15	19.00	-	6
24.11	10.15	11.30	13.00	14.45	16.15	18.00	-	6
25.11	11.30	13.00	17.00	18.30	20.00	-	-	5

Note: The last column determines the number of experiments performed on each given day.

3. Mathematical appendix

A. Complete theory of the branching systems in the frequency domain:

In this appendix, we outline in brief the results obtained previously for the propagation of the blow-like signals in fractal media [14] analyzed previously in the time domain for the complex impedance measured in the frequency domain. We start with the mathematical expression that can describe the complex impedance in fractal media and take into account the branching structure of electric signal/current propagation under the applied voltage.

$$P_N(z) = \prod_{n=-N}^{N} \left(f(z\xi^n)^{n_0 (b(z))^n} \right) = \exp\left[n_0 \sum_{n=-N}^{N} \left(b(z)\right)^n \ln[f(z\xi^n)] \right] \cong \exp S\,(z)$$

$$S(z) = \lim_{N>>1} S_N(z) \tag{1}$$

Here the independent variable $z = i\omega$ is associated with complex frequency, relaxation/transfer the microscopic function $f(z)$ describes the microscopic impedance of some independent block of a complex circuit; the log-periodic function $b(z\xi) = b(z)$ describes a possible branching structure that exists in the complex circuit considered. We take into account the appearance of the branching factor $n_0 b(z)^n$ in the product (1). A schematic model of a branching system is shown in **Figure 4**.

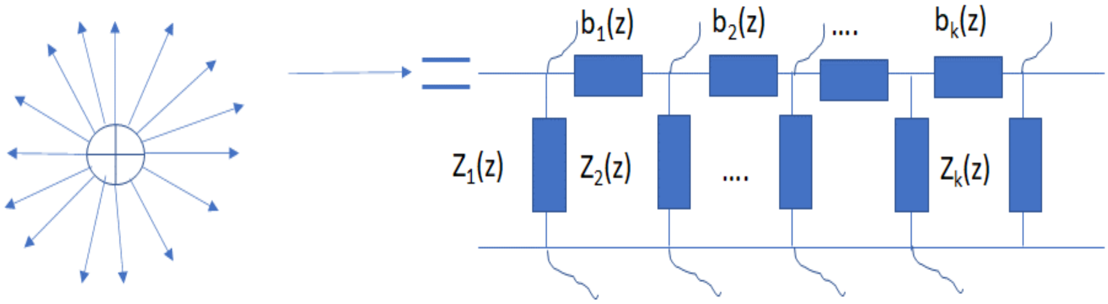

Figure 4. Schematic presentation of a model of a 3D-branching system.

Note: On the left cross-section of the bundle of active electric circuits. The same cross-section of electric circuits forming a connected bundle presents this system on the opposite line. Each arrow represents itself a self-similar fractal circuit or a long line of the Cauer/Forser's type with complex RC elements with nominals $Z_k(z) = Z_0\xi^k$, $b_k(z) = b_0\xi^k$, $(k = 0, 1, 2, \ldots)$. Here ξ is the scaling factor, $z = i\omega$. This relaxation/transfer line has a random length and can be connected randomly with other similar lines, filling all 3D space.

The bio-models considered in detail in the review [15] are presumably in consideration of 2D-plain RC models. Highly likely, the electric circuits corresponding to a large number of bio-models should have distributed conducting channels. Expression (1) can serve as a specific "reflection" of the 3D electric branching structure in the frequency domain. We accept it as the working hypothesis and pay attention to our readers that a possible scenario when this branching or percolation factor is important can be frequently realized in nature. We discuss its significance in the last section. When the branching factor is absent, we obtain the general result discussed in the paper [14].

$$\lim_{N\to\infty} P_N(z) \equiv P(z) = z^{-\nu}\,\Pr\left(\ln(z)\right),$$
$$\nu = \ln\left(\bar{g}\right)/\ln\left(\xi\right), \quad f(z) \overset{\mathrm{Re}(z)>>1}{=} \bar{g}. \tag{2}$$

In expressions (1) and (2), ξ is the scaling factor, $\bar{g}$ is the asymptotic limit of the function $f(z)$ at large values of variable z. As it has been done in the time domain, we want to show that on the intermediate limits of the frequencies, the specific behavior of the microscopic relaxation/transfer function becomes unimportant. Based on its asymptotic behavior, it becomes possible to evaluate the expression (1) and derive a rather general expression. It is suitable for the description of the complex impedances in the intermediate range of frequencies for a wide class of biological systems having a branching structure. This possibility will also be discussed in the last section. We suppose that the microscopic/transfer function has the following asymptotic behavior:

$$Re|z| \ll 1$$
$$f(z) \cong c_1 z^{\alpha} + c_2 z^{1+\alpha} + \cdots \tag{3a}$$
$$f(z) = c_0 + c_1 z + \ldots$$

$$Re|z| \gg 1$$
$$f(z) \cong A_1 z^{-\gamma} exp(-rz) + A_2 z^{-\gamma-1} exp(-2rz) + \cdots \tag{3b}$$

$$f(z) \cong A_0 + A_1 z^{-1} + \ldots$$

In contrast to the asymptotic requirements considered in the paper [14], we chose more general behavior at small and large values of variable z that are given by expressions (3). In the asymptotic behavior of the function $f(z)$ (the first line of (3b)), we consider two possibilities. These are exponential and power-law scenarios, simultaneously. Neglecting the second term in decompositions (3), one can obtain the limiting frequencies that define the mesoscale frequency region where (1) is valid.

$$\omega_{min} \cong \left(min\left(\left|\frac{A_1}{A_0}\right|, \left|\frac{A_2}{A_1}\right| \right) \right) < \omega < \left(max\left(\left|\frac{c_0}{c_1}\right|, \left|\frac{c_1}{c_2}\right| \right) \right) \cong \omega_{max} \tag{4}$$

In expression (4) we took into account both the decompositions in expressions (3a) and (3b), which reflect a branching structure.

At $N >> 1$, the sum $S_N(z)$ can be rewritten as:

$$S_N(z) = n_0 \sum_{n=0}^{N} [b(z)]^n \, ln|f(z\xi^n)| + n_0 \sum_{n=1}^{N} [b(z)]^{-n} \, ln|f(z\xi^{-n})| \tag{5}$$

The second sum by replacement of $1/\xi \to \xi, 1/b(z) \to b(z)$ is reduced to the first sum. Therefore, the second sum can be temporarily omitted. If we put $z\xi \to z$ in the first sum, then one can receive the following equality:

$$S(z\xi) = \frac{1}{b(z)} S(z) - \frac{n_0 \, ln|f(z)|}{b(z)} + n_0 [b(z)]^N \, ln|f(z\xi^{N+1})| \tag{6}$$

We suppose that $b(z\xi) = b(z)$ is a log-periodic function, and it can be presented by the log-periodic decomposition. Therefore, the log-periodic function $b(z)$ is limited and lies in the interval:

$$b(z) = bc_0 + \sum_{k=1}^{K} [bc_k \, cos(\Omega_k \, ln\, z) + bs_k \, sin(\Omega_k \, ln\, z)],$$

$$\Omega_k = \frac{2\pi \cdot k}{ln\, \xi} \tag{7a}$$

$$|b(z)| \leq max\, b\,(z) - min\, b\,(z) \equiv Range(b(z)) = b_R \tag{7b}$$

If $|b_R| < 1$, then the contribution of the last term in (6) will be very small for any values of z. Taking into account the asymptotic values of the function $f(z)$ at small and large values of z, we obtain the functional equation as in (8). This is valid for the intermediate range of scales.

$$S(z\xi) = \frac{1}{b(z)} S(z) + \mu \, ln(\, z) + gz + X_0 \tag{8}$$

where the parameters μ, g, and X_0 are defined by the following expressions:

$$\mu = -n_0 \left(\frac{\alpha}{b_{min} \frac{\gamma}{b_{max}}}, g = -\frac{n_0 r}{b_{max_0} \, ln\left(\frac{c_1 A_1}{bmin_{max}}\right)} \right) \tag{9}$$

The solution of Equation (8) obtained with the help of the uncertain coefficients method can be written as:

$$\begin{aligned}
&S(z) = z^{\nu(z)}\, Pr(\ln z) + C_1(z)\ln z + C_2(z)\cdot z + C_3(z),\\
&C_1(z) = \frac{\mu}{1-1/b(z)}, C_2(z) = \frac{g}{\xi - 1/b(z)}, C_3(z) = \frac{X_0 - C_1(z)\ln\xi}{1-1/b(z)},\\
&\nu(z) = -\frac{\ln\big(b(z)\big)}{\ln\xi}, b(z\xi) = b(z).
\end{aligned} \tag{10}$$

In this paper, based on the minimal values of the fitting errors (the order of it is 0.1%), we chose the solution of (A10) as the fitting function by replacing $b(z) \to b_{\mathrm{eff}}$. This effective value for each experiment can be found find from the fitting procedure explained below. The proposed fitting function can be written as:

$$\begin{aligned}
&S(z) = z^{\nu}\, Pr(\ln z) + C_1\ln z + C_2 z + C_3,\\
&C_1 = \frac{\mu}{1-1/b_{eff}}, C_2 = \frac{g}{\xi - 1/b_{eff}}, C_3 = \frac{X_0 - C_1\ln\xi}{1-1/b_{eff}},\\
&\nu = -\frac{\ln\big(b_{eff}\big)}{\ln\xi}.
\end{aligned} \tag{11}$$

Here $Pr(\ln\, z)$ is the log-periodic function that is defined by the following expression:

$$\begin{aligned}
&Pr(\ln z) = Ac_0 + \sum_{k=1}^{K}\left[Ac_k\cos(\Omega_k\ln z) + As_k\sin(\Omega_k\ln z)\right],\\
&\Omega_k = \frac{2\pi\cdot k}{\ln\xi}, Pr(\ln z \pm \ln\xi) = Pr(\ln z).
\end{aligned} \tag{12}$$

Taking into account the value of the complex variable $z = i\omega$, and selecting the real and imaginary parts from (11) and (12), we get the following expressions:

$$\begin{aligned}
&Re(S(i\omega)) = \exp(\nu x)\left[A_0 + \sum_{k=1}^{K}\big(Ac_k\cos(\Omega_k x) + As_k\sin(\Omega_k x)\big)\right] + C_1 x + C_3,\\
&Im(S(i\omega)) = \left(\frac{\pi}{2}C_1\right) + \exp(\nu x)\left[\sum_{k=1}^{K}\big(AC_k\cos(\Omega_k x) + AS_k\sin(\Omega_k x)\big)\right] + C_2\exp(x),\\
&\Omega_k = \frac{2\pi\cdot k}{\ln\xi}, x = \ln\omega.
\end{aligned} \tag{13}$$

We will choose the hypothesis providing the most accurate fit with a minimal number of K. After realization of the fitting of expressions in (13), the final fit is expressed as:

$$\begin{aligned}
&Re\big(Z(\omega)\big) - i\, Im\big(Z(\omega)\big) =\\
&= \exp\big(Re\, S\,(i\omega)\big) - i\exp\big(Im\, S\,(i\omega)\big)
\end{aligned} \tag{14}$$

The proposed algorithm is reduced to the initial fit of the real part $\mathrm{Re}(S(i\omega))$. After evaluation of the fitting constants C_1, C_2, and C_3, one can fit the function $\mathrm{Im}(S(i\omega))$. Five key fitting parameters ν, C_1, C_2, C_3, and $\Omega_1 = 2\pi/\ln(\xi)$ can be calculated from (13). This allows us to evaluate the asymptotic values of the function

$f(z)$ figuring in (3), and the value of the b_{eff} becomes,

$$\begin{gathered} b_{eff} = exp(-\nu \, ln \, \xi) \\ D_{\alpha\gamma} \equiv \alpha - \gamma = \frac{C_1}{2}\left(1 - b_{eff}\right), at n_0 \cong 2, \\ X_0 = C_1 \, ln \, \xi + C_3\left(1 - \frac{1}{b_{eff}}\right) \\ rn_0 = C_2\left(1 - \xi b_{eff}\right). \end{gathered} \tag{15}$$

For obtaining these expressions, we replace minimal and maximal values of $b_{\min,\max}$ by its effective parameter b_{eff} in expressions (9). It will be evaluated from the fitting procedure. Expression (15) allows us to evaluate the difference between the power-law exponents $D_{\alpha\gamma}$, the values of the X_0, and parameter r that enter the asymptotic decompositions (3).

We should highlight here the meaning of the parameters that figured in expression (15). The basic power-law parameter, ν reflects the fractal dynamic structure that is formed by percolation currents. Two other power-law parameters, α and γ determine the dynamic size of the structure at small and large frequencies, correspondingly. Parameter, ξ determines the value of the scaling factor, and parameter, n_0 determines the number of possible neighbors in the percolation system that enable the conduction of an electric current. Actually, we found a general mechanism for conducting electric current in a wide class of living systems, such as leaves and mushrooms. In this paper cocoons also form a specific branching system, as well.

Besides the fitting constants, the coefficients are evaluated by the linear least square method (LLSM). We cannot show them for all the 76 experiments (see **Table 1**). However, one can select the most interesting temporal stages of the cocoon impedance evolution. We analyze 6 measurements reflecting the evolution of the impedance data. We select three experiments: from the first block we choose day 15.11 (11.00 (m = 1), 17.45 (m = 5)), from the second block 17.11 (10.45 (m = 1), 17.15 (m = 5)) and, finally, from the third block 23.11 (10.00 (m = 1), 17.15 (m = 5)). We note also that the measured impedance at the beginning of each day (m = 1) has a monotone character. At the end of the day, the monotone behavior is destroyed (m = 5) and replaced by a chaotic character. However, the proposed branching model enables us to fit these data with high accuracy, including the chaotic behavior as well.

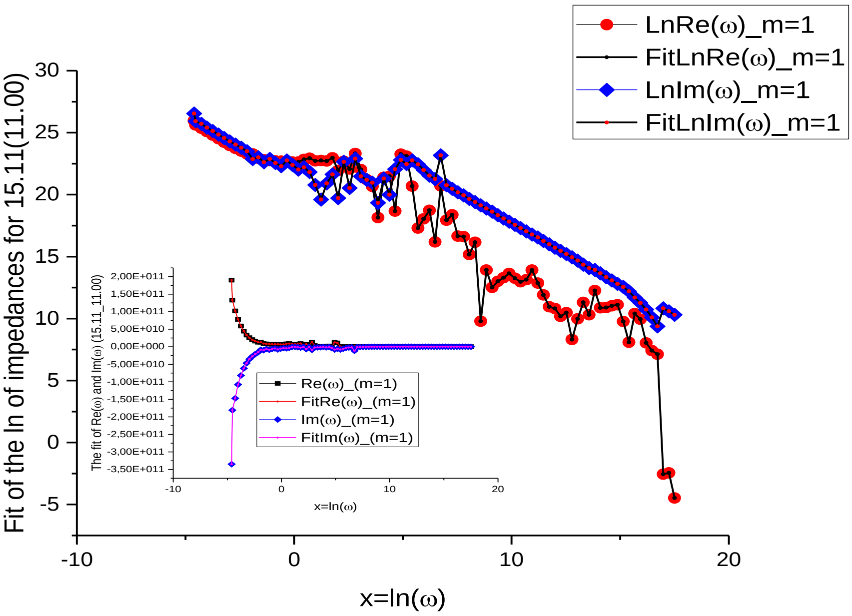

Figure 5. Fit of the real and imaginary parts of the impedances corresponding to the beginning of the experiment on 15.11.2023.

Figure 5 demonstrates the fit of the real and imaginary parts of the impedances corresponding to the beginning of the experiment on 15.11 at 11.00 AM. In the central figure, we demonstrate the fit of the functions expressed in the form of the natural logarithm (13). On the small figure (taking into account the negative sign), we show the fit of the measured impedances in a semi-logarithmic scale. As one can notice from this figure, the behavior of the measured impedances looks like a monotone function.

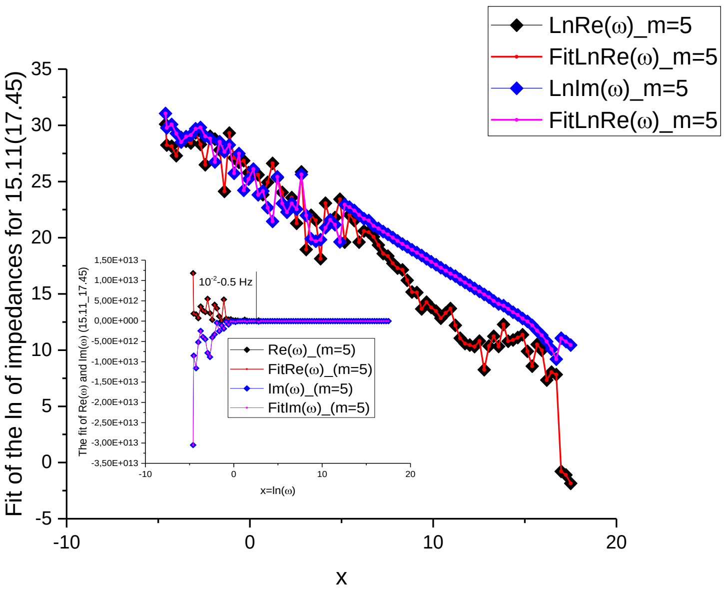

Figure 6. Fit of the real and imaginary parts of the impedances corresponding to the 5th experiment on 15.11.2023.

Figure 6 demonstrates the fit of the real and imaginary parts of the impedances corresponding to the 5th experiment on 15.11 (17.45_m = 5). In the central figure, we demonstrate the fit of the functions expressed in the form of the natural logarithm (13). On the small figure (taking into account the negative sign), we show the fit of the measured impedances in a semi-logarithmic scale. One can notice from this figure that the behavior of the measured impedances is changed considerably. In the range of small frequencies (10^{-2}–0.5 Hz) the curves look chaotic; however, the proposed model provides an accurate fit.

The dependence of the modulus values for real and imaginary parts of $Z(\omega)$ are shown in **Figure 7**. Whereas, the dependence of phase values for real and imaginary parts is shown in **Figure 8**.

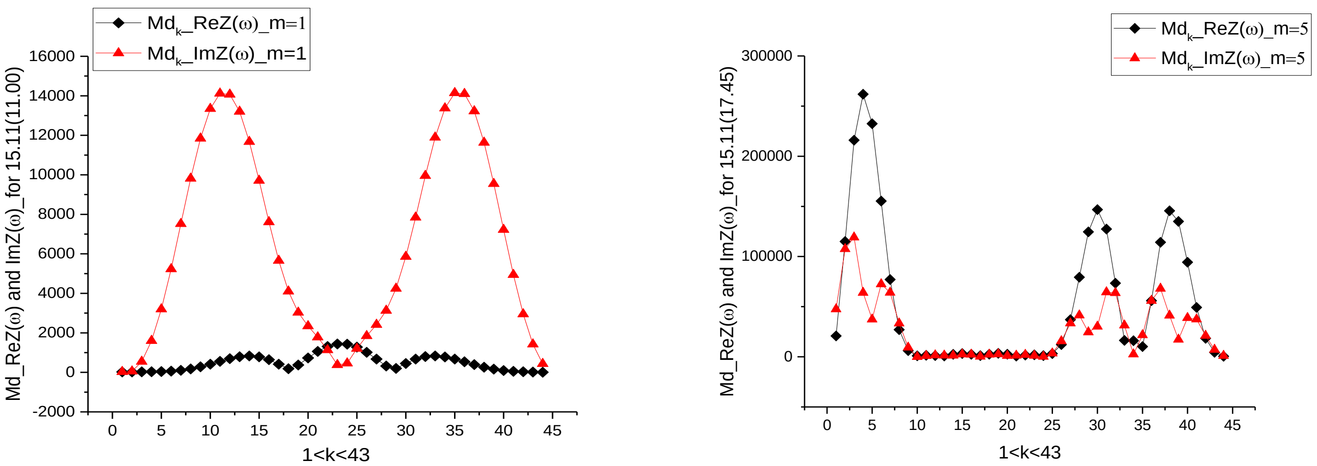

(a) **(b)**

Figure 7. The dependence of the modulus values. **(a)** For real and imaginary parts of $Z(\omega)$ corresponds to the experiment performed on 15.11 (11.00_m = 1); **(b)** for real and imaginary parts of $Z(\omega)$ corresponds to the experiment performed on 15.11 (17.45_m = 5).

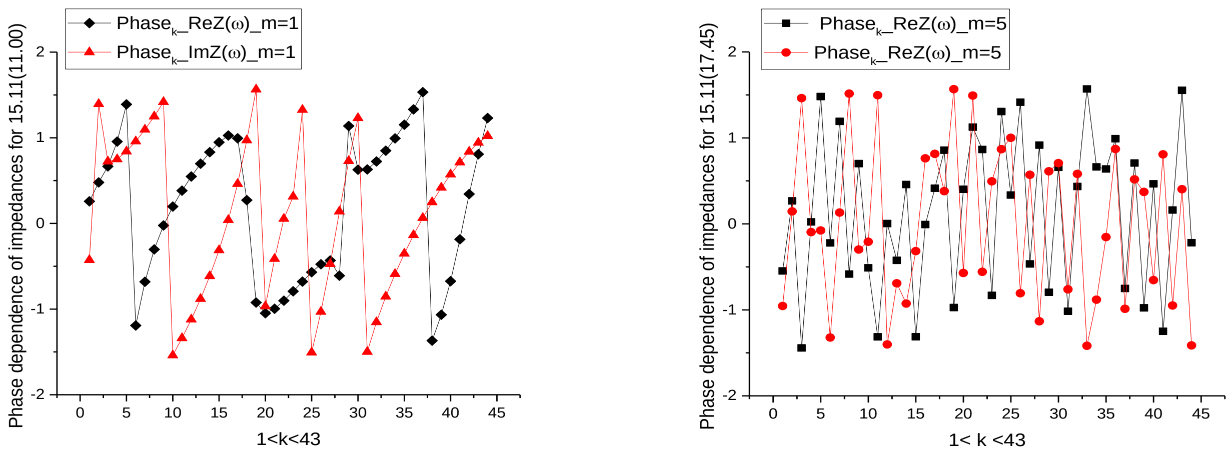

(a) **(b)**

Figure 8. The dependence of the phase values. **(a)** For real and imaginary parts of $Z(\omega)$ corresponding to the experiment performed on 15.11 (11.00_m = 1); **(b)** for real and imaginary parts of $Z(\omega)$ corresponding to the experiment performed on 15.11 (17.45_m = 5).

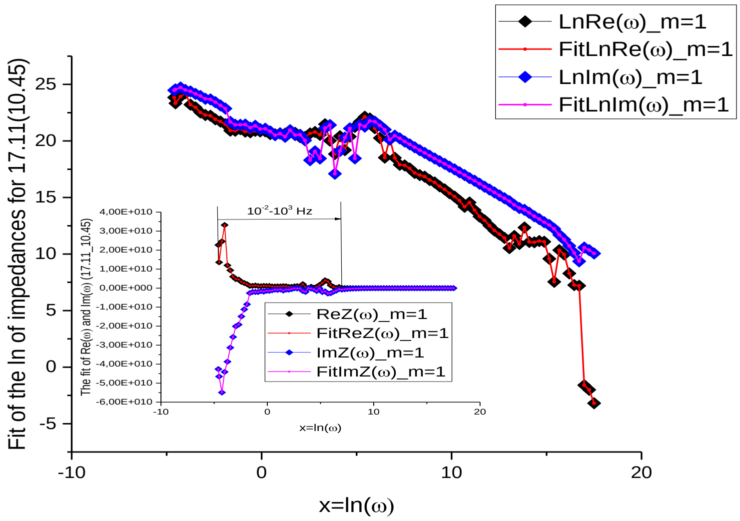

Figure 9. Fit of the real and imaginary parts of the impedances corresponding to the beginning of the experiment on 17.11.2023.

Figure 9 demonstrates the fit of the real and imaginary parts of the impedances corresponding to the 1st experiment on 17.11 at 10.45 AM. In the central figure, we demonstrate the fit of the functions expressed in the form of the natural logarithm (13). On the small figure (taking into account the negative sign), we show the fit of the measured impedances in a semi-logarithmic scale. One can notice from this figure that the behavior of the measured impedances has changed considerably. In the range of small frequencies (10^{-2}–10^{3} Hz), the curves look monotone, and the proposed model provides an accurate fit.

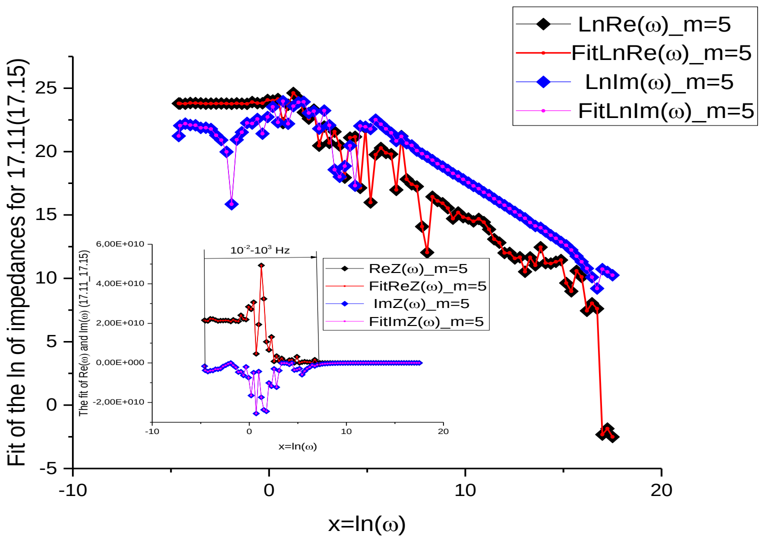

Figure 10. Fit of the real and imaginary parts of the impedances corresponding to the 5th experiment on 17.11.2023.

Figure 10 demonstrates the fit of the real and imaginary parts of the impedances corresponding to the 5th experiment on 17.11.2023. In the central figure, we demonstrate the fit of the functions expressed in the form of the natural logarithm (13). On the small figure (taking into account the negative sign), we show the fit of the measured impedances in a semi-logarithmic scale. One can notice from this figure that the behavior of the measured impedances has changed considerably. In the range of small frequencies (10^{-2}–10^3 Hz), the curves look chaotic, and the proposed model provides an accurate fit.

Figures 11 and **12** show the dependence of the modulus and phase values for the measurement on 17.11.2023.

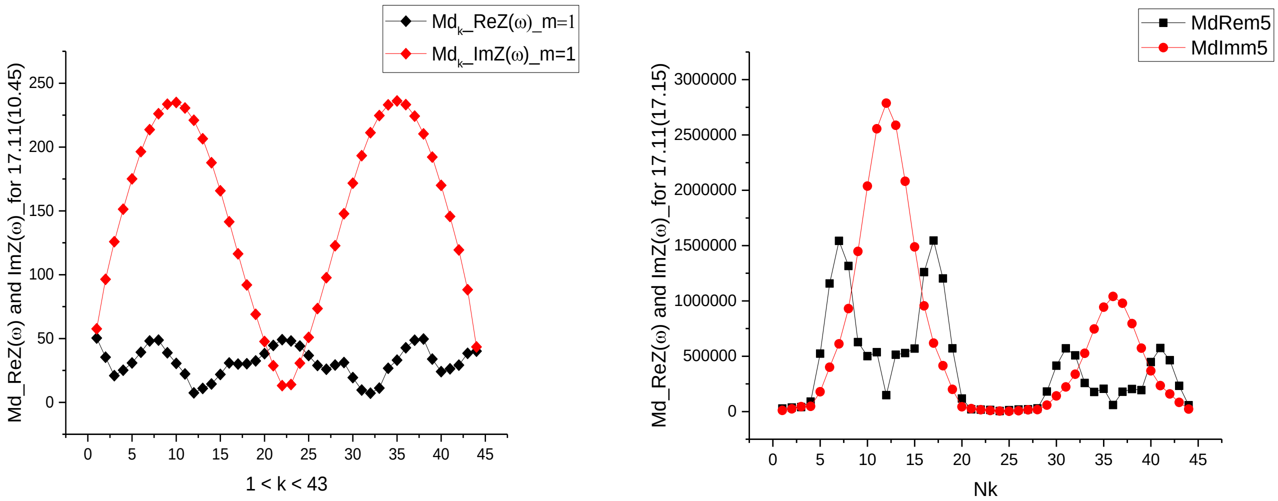

(a) **(b)**

Figure 11. The dependence of the modulus values $Md_k = \sqrt{Ac_k^2 + As_k^2}$. (a) For real and imaginary parts of $Z(\omega)$ corresponding to the experiment performed on 17.11 (10.45_m = 1); **(b)** for real and imaginary parts of $Z(\omega)$ corresponding to the experiment performed on 17.11 (17.15_m = 5).

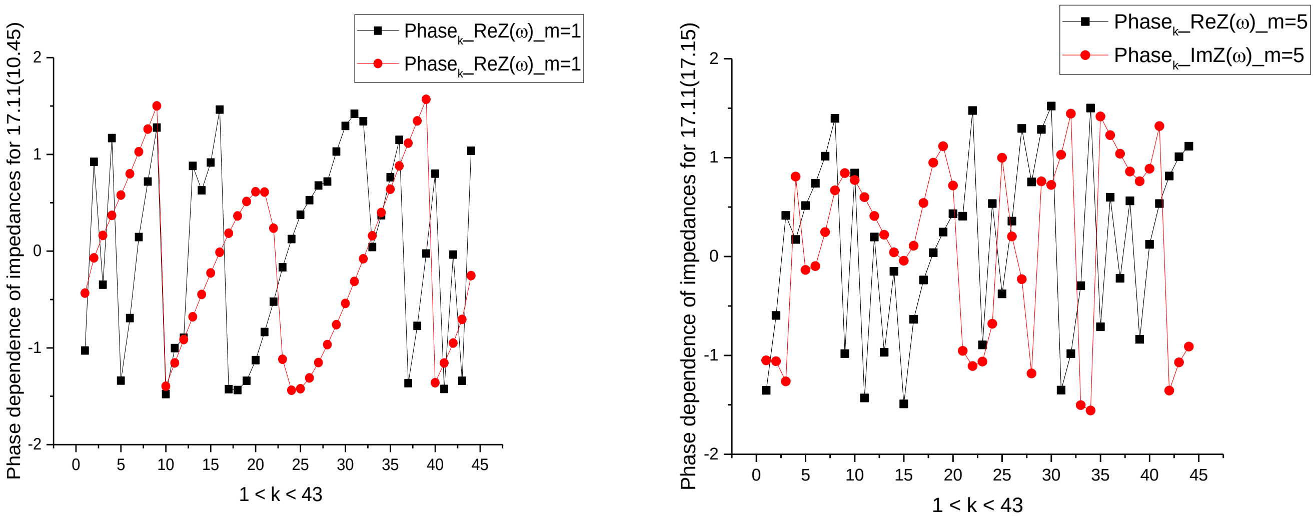

(a) **(b)**

Figure 12. The dependence of the phase $Ph_k = \tan^{-1}\left(\frac{As_k}{Ac_k}\right)$ values. **(a)** For real and imaginary parts of $Z(\omega)$ corresponds to the experiment performed on 17.11 (10.45_m = 1); **(b** for real and imaginary parts of $Z(\omega)$ corresponds to the experiment performed on 17.11 (17.15_m = 5).

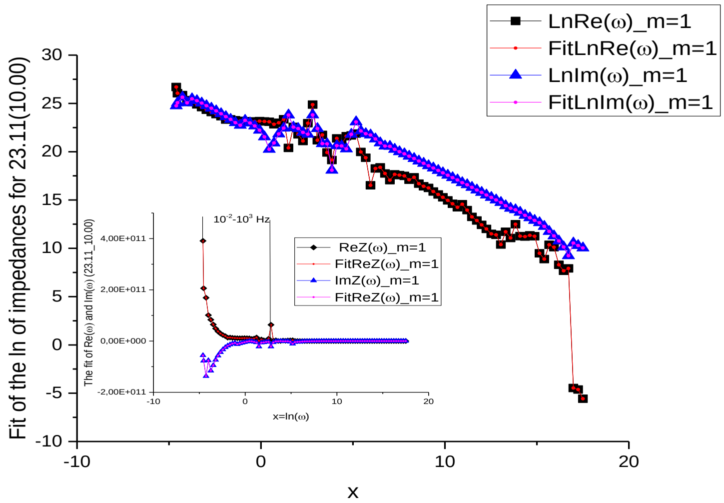

Figure 13. Fit of the real and imaginary parts of the impedances corresponding to the beginning of the experiment on 23.11.2023.

Figure 13 demonstrates the fit of the real and imaginary parts of the impedances corresponding to the 1st experiment on 23.11. 2023 at 10.00 AM. In the central figure, we demonstrate the fit of the functions expressed in the form of the natural logarithm (13). On the small figure (taking into account the negative sign), we show the fit of the measured impedances in a semi-logarithmic scale. One can notice from this figure that the behavior of the measured impedances is changed considerably. In the range of small frequencies (10^{-2}–10^{3} Hz), the curves look as monotone, and the proposed model provides an accurate fit.

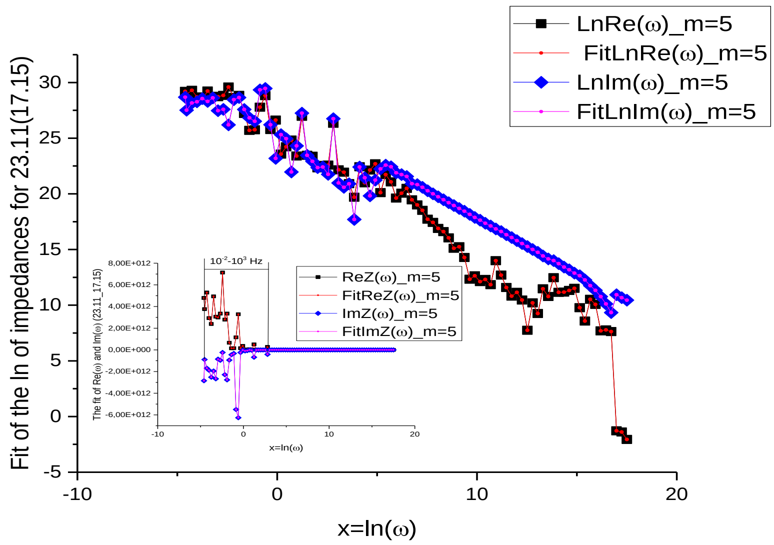

Figure 14. Fit of the real and imaginary parts of the impedances corresponding to the 5th experiment on 23.11.2023.

Figure 14 demonstrates the fit of the real and imaginary parts of the impedances corresponding to the 5th experiment on 23.11 (17.15_*m* = 5). In the central figure, we demonstrate the fit of the functions expressed as the natural logarithm (13). On the small figure (considering the negative sign), we show the fit of the measured impedances in a semi-logarithmic scale. It can be noticed from this figure that the behavior of the measured impedances is chaotic in nature in the frequency range (10^{-2}–10^{3} Hz). However, the proposed model provides an accurate fit.

4. Analysis of the measured data and discussion of the obtained results

The question is, how to understand the impedance behavior of the measured cocoon (at least qualitatively) based on an analysis of the total set of 76 experiments?

We suppose that the structure of a living cocoon is similar to some complicated heterogeneous semiconducting structure and contains a random system of open/closed channels. All experiments can be divided approximately into three stages. For the separation of these stages, we use **Figure 1**, where the range distribution of all the impedances is shown. We notice the following peculiarity in the analysis of these measured impedances. At the beginning of each measurement of a particular day, the impedance has a monotone character (see the fit of impedance curves in double log scale in the central figures 5, 9, 13). On the same small figures, we demonstrate the fit of impedances in the semi-log scale. In **Figures 6**, **10**, and **14**, we show the quasi-chaotic behavior for the impedances realized at the end of the day. This peculiarity allows us to conclude that the applied external voltage strongly disturbs the internal processes that take place in the transformation of the cocoon into the adult moth. This peculiarity is confirmed by the set of **Figures 7a**,**b**, and **8a**,**b** and **11a**,**b** and **12a**,**b** and **15a**,**b** and **16a**,**b**. In these figures, the frequency responses (modulus and phases) are shown for the beginning (m = 1) and at the end (m = 5) of the measurement on a particular day. One can notice that for m = 1, these dependences are not chaotic, while for m = 5, these dependences are chaotic. On the figures from 17 to 20, we demonstrate the calculated parameters: $\Omega_1(N)$ (**Figure 17**), $C_1(N)$ (**Figure 18**), $\nu(N)$ (**Figure 19**), $D_{\alpha\gamma}(N)$ (**Figure 20**). The parameters are evaluated from the Equation (15).

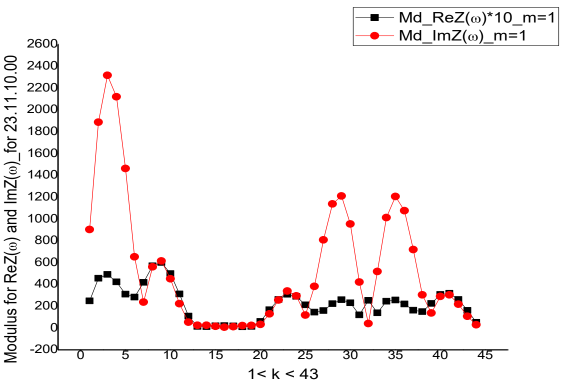

(a)

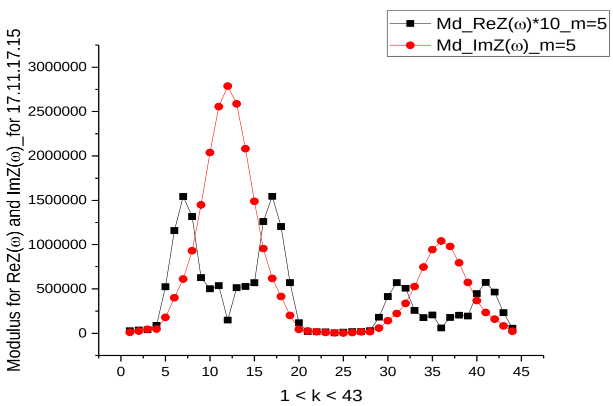

(b)

Figure 15. The dependence of the modulus $Md_k = \sqrt{Ac_k^2 + As_k^2}$ values. **(a)** For real and imaginary parts of $Z(\omega)$ corresponds to the experiment performed on 23.11 (10.00_m = 1); **(b)** for real and imaginary parts of $Z(\omega)$ corresponds to the experiment performed on 23.11 (17.15_m = 5).

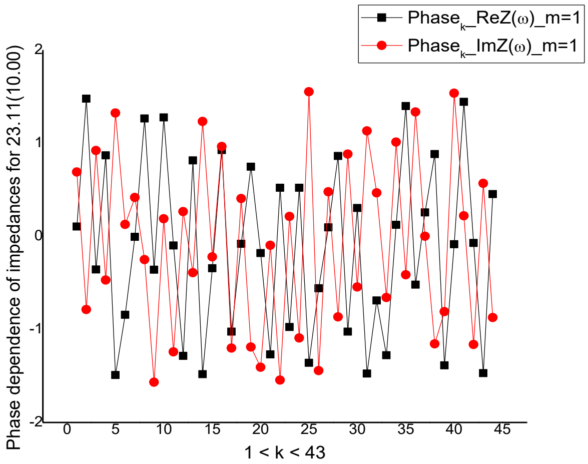

(a)

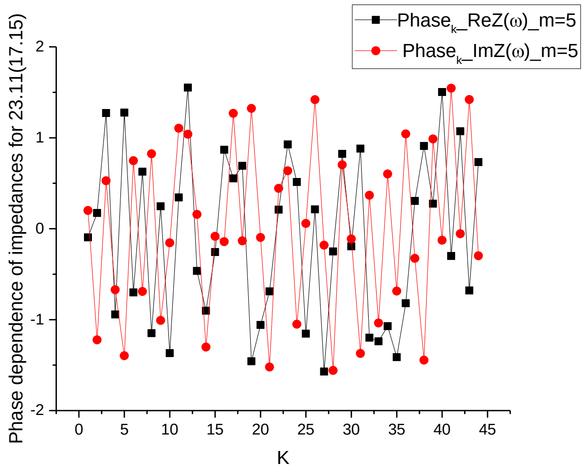

(b)

Figure 16. The dependence of the phase values $Ph_k = \tan^{-1}\left(\frac{As_k}{Ac_k}\right)$**. (a)** For real and imaginary parts of $Z(\omega)$ corresponds to the experiment performed on 23.11 (10.00_m = 1); **(b)** for real and imaginary parts of $Z(\omega)$ corresponds to the experiment performed on 23.11 (17.15_m = 5).

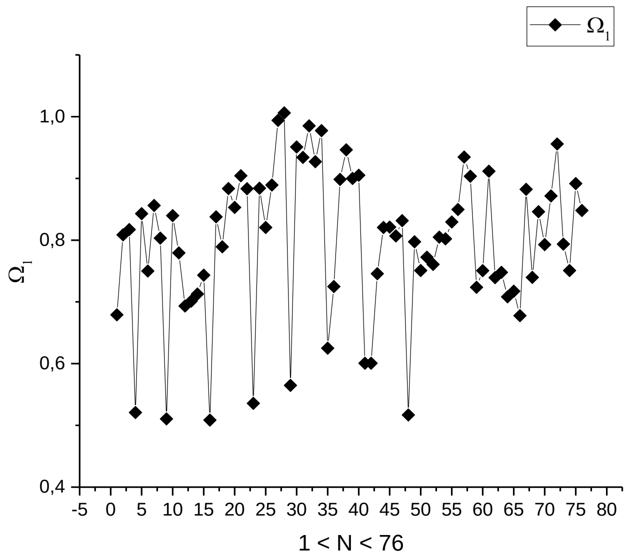

Figure 17. The distribution of the frequencies $\Omega_1 = 2\pi/\ln\xi$ over all 76 experiments.

As one can see from this figure, the behavior of these frequencies is not monotone. This frequency distribution is located in the interval $0.51 < \Omega_1 < 1.0$.

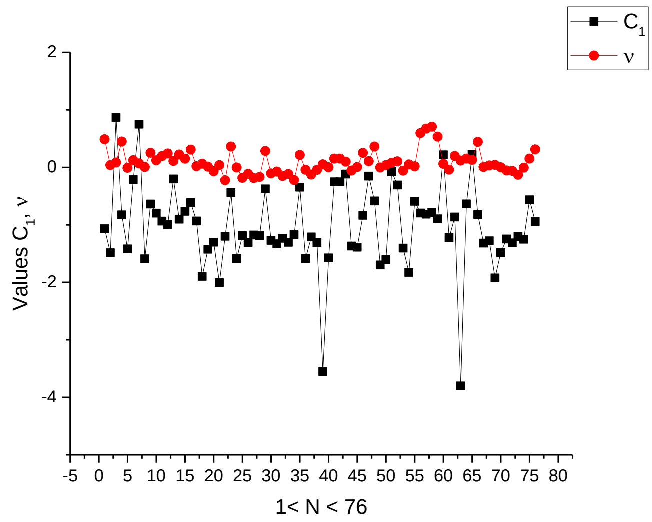

Figure 18. The distribution of the fitting parameter C_1 and power-law exponent (ν).

This figure shows two distributions. Parameter C_1 (playing the role of the power law exponent that stands before the exponential function; see expression (10)) and power-law exponent (ν). The interval for these exponents is for C_1 [−3.801, 0.868] and ν [−0.225, 0.707]. Again, one can say that the behavior of these distributions has a non-monotone character.

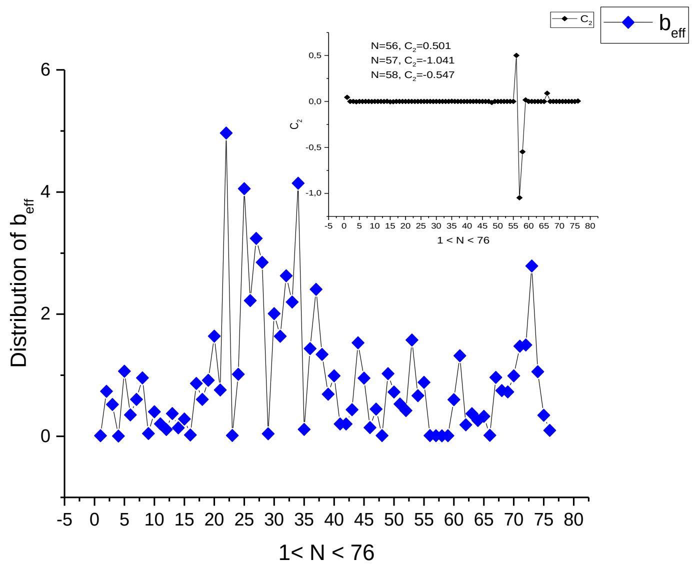

Figure 19. The distribution of the parameters b_{eff} and C_2

The distribution of the b_{eff} on the central figure and parameter C_2 on the small figure above. Parameter C_2 accepts small values except for a group of measurements associated with 56–59 experiments. This anomaly cannot be explained properly. The parameter b_{eff} increases in the interval [21,34], for other measurements, it is close to the unit value except for the 73rd measurement. Three stages can be seen clearly. The most intensive stage covers the range of 15–40 experiments. Highly likely, this stage reflects the most intensive stage in dynamic fractal behavior.

Parameter C_2 accepts small values except for a group of measurements associated with 56–59 experiments. This anomaly cannot be explained properly as no direct measurement can be performed. However, on the 10th day of measurement (56–59), the moth came out of the shell, and hence, a different behavior was observed.

The parameter b_{eff} increases in the interval [21,34], this is the 3rd to 6th day of the experiment, and intuitively we can say that at this time the pupa inside the cocoon may undergo drastic change. But for a confirmed conclusion, further investigation is required.

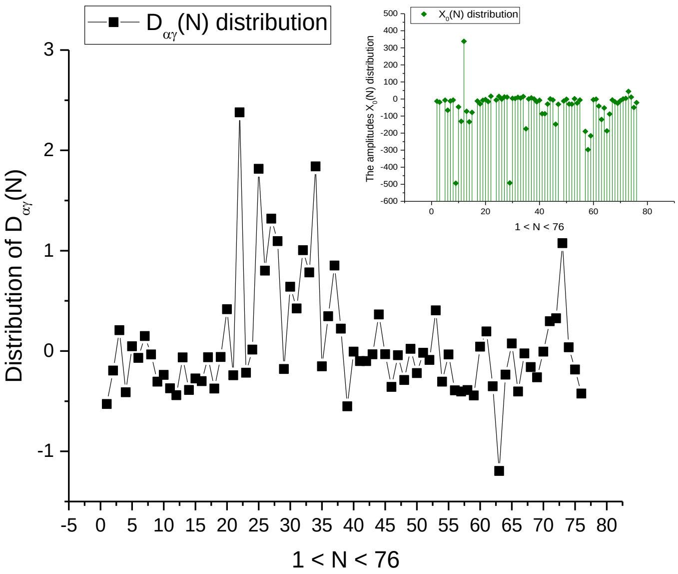

Figure 20. Distributions of the parameter $D_{\alpha\gamma}(N)$.

This figure demonstrates two important distributions, $D_{\alpha\gamma}(N)$ (on the central figure) and $X_0(N)$, that are evaluated from (15). It is similar to the previous figure, and the power-law parameters and γ reflect the basic stages of the dynamic evolution of the percolation phenomenon that takes place inside a cocoon.

All figures (more or less) reflect the common scenario—percolation of the current over a random set of branching channels. Some specific details are reflected by the specific figures. It depends on the conducting structure of the cocoon.

We would like to note that a large number of works can be found in the literature on geometric fractals. Rami Ahmad El-Nabulsi worked on the dynamical properties of anisotropic media [16,17] and Chen on urban geometry [18,19]. He et al. has described the energy bands using fractals in electronic systems to quantize bulk dipole and quadrupole moments in crystalline structures [20]. Mittal et al. realized a topological system using a 2D lattice of nanophotonic silicon ring resonators and claim that this provides robust on-chip topological protection [21]. Shimada et al. worked on the Ising model in non-integer dimensions [22].

Unlike fractal geometry, which is static in nature, the present work is on the analysis of fractal structure, which is formed inside the cocoon due to the conduction of current. The paper also provides a mathematical expression that can describe the complex impedance in fractal media and take into account the branching structure of electric signal/current propagation under the applied voltage.

Some of the works also can be found on the bio-impedance model of living systems [23,24]. However, in this paper, the main emphasis is on the formation of fractal structures in a living system due to the conduction of signals, which is dynamic in nature.

5. Conclusion

The paper presents a 3D structured conducting channel inside the cocoon during its transformation from pupa to moth. A mathematical model of the 3D branching is explained with the complex conjugated power law of exponents.

The basic conclusions can be summarized as:

(1) Discovery of a new fractal element with complex-conjugated power-law exponents that can exist in living systems.
(2) The proposed theory of the blow-like signals was applied successfully in the frequency domain for the description of the evolution of a 3D-branching system as a cocoon.
(3) All measured data (even including outliers) are fitted completely to the proposed fitting functions with a value of a relative error of less than 0.1%.
(4) We give a qualitative explanation of the conductive processes that do not contradict the measured impedance data.
(5) Three stages can be seen clearly by analyzing the experimental data. The most intensive stage covers the range from experiment no. 15 to 40. These stages reflect the most intensive stage in dynamic fractal behavior. In other words, from the 3rd to the 6th day of the experiment, the cocoon displays rigorous change.
(6) We discovered a general scenario for the random distribution of the current in 3D-living systems. Based on our previous results, one can say that the random currents are distributed over conducting channels, and these channels can be approximately characterized by the parameters that are given by relationships (15). These parameters can characterize approximately the fractal structure that is dynamic in nature and provides the current distribution over the formed branching structure.

Author contributions: Conceptualization, RRN and KB; methodology, KB; software, RRN; validation, RRN and KB; formal analysis, RRN; investigation, KB; resources, KB; data curation, KB; writing—original draft preparation, MC; writing—review and editing, KB and MC; visualization, MC; supervision, RRN and KB; project administration, RRN; funding acquisition, RRN. All authors have read and agreed to the published version of the manuscript.

Acknowledgments: The authors gratefully acknowledge the support from Arun Kumar Das of Debra Sericulture complex who has supplied the cocoons unconditionally to carry out the experiments. The authors would also like to express their sincere gratitude to Avijit Mondal and Indrani Ray for their invaluable assistance during the experimental work. One of us (RRN) would like to emphasize that this work was written as part of project 20–30, which was approved by the top universities in Russian Federation.

Institutional review board statement: Not applicable.

Informed consent statement: Not applicable.

Conflict of interest: The authors declare no conflict of interest.

References

1. Nigmatullin R, Sarkar S, Biswas K. The Detection of Self-Similar/Branching Processes in Complex Biological Systems: Analysis of the Temporal Evolution of Impedance Measurements in Tulsi (Holy Basil) Leaves "Ocimumtenuiflorum." IEEE/ACM Transactions on Computational Biology and Bioinformatics. 2022; 19(5): 3038-3047. doi: 10.1109/tcbb.2021.3107323
2. Nigmatullin RR, Sarkar S, Biswas K. Detection of a fractal element with complex-conjugated power-law exponents in living systems: Analysis of the temporal evolution of impedance measurements in the unblown bud plumeria flower (frangipani plumeria). In: International workshop on Advanced Theory and Applications of Fractional Calculus. Springer; 2021. pp. 118–124.
3. Chen F, Porter D, Vollrath F. Structure and physical properties of silkworm cocoons. Journal of The Royal Society Interface. 2012; 9(74): 2299-2308. doi: 10.1098/rsif.2011.0887
4. Rahmathulla VK. Management of Climatic Factors for Successful Silkworm (Bombyx moriL.) Crop and Higher Silk Production: A Review. Psyche: A Journal of Entomology. 2012; 2012: 1-12. doi: 10.1155/2012/121234
5. Ashraf H, Qamar A. Silkworm Bombyx mori as a model organism: A review. Physiological Entomology. 2023; 48(4): 107-121. doi: 10.1111/phen.12421
6. Lü P, Pan Y, Yang Y, et al. Discovery of anti-viral molecules and their vital functions in Bombyx mori. Journal of Invertebrate Pathology. 2018; 154: 12-18. doi: 10.1016/j.jip.2018.02.012
7. Marzoli F, Antonelli P, Saviane A, et al. Bombyx mori from a food safety perspective: A systematic review. Food Research International. 2022; 160: 111679. doi: 10.1016/j.foodres.2022.111679
8. Montali A, Berini F, Saviane A, et al. A Bombyx mori Infection Model for Screening Antibiotics against Staphylococcus epidermidis. Insects. 2022; 13(8): 748. doi: 10.3390/insects13080748
9. Abdelli N, Peng L, Keping C. Silkworm, Bombyx mori, as an alternative model organism in toxicological research. Environmental Science and Pollution Research. 2018; 25(35): 35048-35054. doi: 10.1007/s11356-018-3442-8
10. Muhammad A, Qian Z, Li Y, et al. Enhanced bioaccumulation and toxicity of Fenpropathrin by polystyrene nano(micro)plastics in the model insect, silkworm (Bombyx mori). Journal of Nanobiotechnology. 2025; 23(1). doi: 10.1186/s12951-025-03120-8
11. Tulachan B, Meena SK, Rai RK, et al. Electricity from the Silk Cocoon Membrane. Scientific Reports. 2014; 4(1). doi: 10.1038/srep05434
12. Liu J, Shi L, Deng Y, et al. Silk sericin-based materials for biomedical applications. Biomaterials. 2022; 287: 121638. doi: 10.1016/j.biomaterials.2022.121638
13. Leal-Egaña A, Scheibel T. Silk-based materials for biomedical applications. Biotechnology and Applied Biochemistry. 2010; 55(3): 155-167. doi: 10.1042/ba20090229
14. Nigmatullin RR, Toboev VA, Lino P, et al. Reduced fractal model for quantitative analysis of averaged micromotions in mesoscale: Characterization of blow-like signals. Chaos, Solitons & Fractals. 2015; 76: 166-181. doi: 10.1016/j.chaos.2015.03.022
15. Nigmatullin RR, Mehaute AL. Is there geometrical/physical meaning of the fractional integral with complex exponent? Journal of Non-Crystalline Solids. 2005; 351(33-36): 2888-2899. doi: 10.1016/j.jnoncrysol.2005.05.035
16. El-Nabulsi RA. Modelling nematic liquid crystal in fractal dimensions. Medicine in Novel Technology and Devices. 2024; 24: 100334. doi: 10.1016/j.medntd.2024.100334
17. El-Nabulsi RA. Fractal Pennes and Cattaneo–Vernotte bioheat equations from product-like fractal geometry and their implications on cells in the presence of tumour growth. Journal of The Royal Society Interface. 2021; 18(182): 20210564. doi: 10.1098/rsif.2021.0564
18. Chen Y. Fractal Modeling and Fractal Dimension Description of Urban Morphology. Entropy. 2020; 22(9): 961. doi: 10.3390/e22090961

19. Chen Y. Two Sets of Simple Formulae to Estimating Fractal Dimension of Irregular Boundaries. Mathematical Problems in Engineering. 2020; 2020: 1-15. doi: 10.1155/2020/7528703
20. He L, Addison Z, Mele EJ, et al. Quadrupole topological photonic crystals. Nature Communications. 2020; 11(1). doi: 10.1038/s41467-020-16916-z
21. Mittal S, Orre VV, Zhu G, et al. Photonic quadrupole topological phases. Nature Photonics. 2019; 13(10): 692-696. doi: 10.1038/s41566-019-0452-0
22. Shimada H, Hikami S. Fractal Dimensions of Self-Avoiding Walks and Ising High-Temperature Graphs in 3D Conformal Bootstrap. Journal of Statistical Physics. 2016; 165(6): 1006-1035. doi: 10.1007/s10955-016-1658-x
23. Mohsen M, Said LA, Madian AH, et al. Fractional-Order Bio-Impedance Modeling for Interdisciplinary Applications: A Review. IEEE Access. 2021; 9: 33158-33168. doi: 10.1109/access.2021.3059963
24. Lopes AM, Machado JT. Modeling vegetable fractals by means of fractional-order equations. Journal of Vibration and Control. 2015; 22(8): 2100-2108. doi: 10.1177/1077546315581228